Wind-driven Circulation in Estuaries and Bays

Clinton Winant

June 11, 2023

Chapter 1

A Shallow Wind Driven Lake

1.1 The model

Consider a closed basin filled with fluid, similar to the one sketched in figure. 1.1. The wind, blowing over the basin, imposes a stress vector of amplitude τ^{*1} on the surface of the water. The dimensional length of the basin is $2L^*$ and the width is $2B^*$. The maximum depth is H^* and the local depth, normalized by the maximum depth ($0 \leq h(x, y) \leq 1$. We begin by looking for steady flow ($\partial/\partial t = 0$), and neglect the efects of advection on the momentum equations. The linearized mass and momentum equations are the solved, assuming the pressure is hydrostatic. In terms of dimensional variables, the governing equations and boundary conditions include the mass conservation equation:

$$\frac{\partial u^*}{\partial x^*} + \frac{\partial v^*}{\partial y^*} + \frac{\partial w^*}{\partial z^*}, \tag{1.1}$$

the two components of the horizontal momentum equations:

$$\frac{\partial p^*}{\partial x^*} = \rho^* K_v^* \left(\frac{\partial^2 u^*}{\partial x^{*2}} + \frac{\partial^2 u^*}{\partial y^{*2}} + \frac{\partial^2 u^*}{\partial z^{*2}} \right); \tag{1.2}$$

[1] dimensional variables are denoted by an asterisk

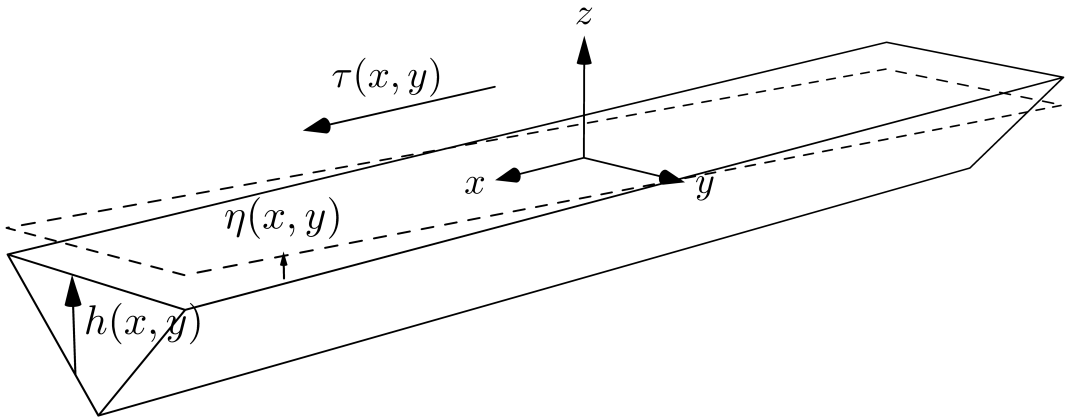

Figure 1.1: Sketch of an idealized lake or closed basin. Wind blows over the surface, in this case parallel to the x axis. The undisturbed sea level defines the $z = 0$ plane. The wind causes the surface to rise by an amount $\eta(x, y)$. The local water depth normalized by the maximum depth is $h(v, y)$. (made with asy)

$$\frac{\partial p^*}{\partial y^*} = \rho^* K_v^* \left(\frac{\partial^2 v^*}{\partial x^{*2}} + \frac{\partial^2 v^*}{\partial y^{*2}} + \frac{\partial^2 v^*}{\partial z^{*2}} \right) \tag{1.3}$$

here is the constant density and K_v^* is the vertical eddy diffusivity. Typically, in estuaries $K_v^* \approx 10^{-3} m^2 s^{-1}$.

Because vertical velocities are expected to be much smaller than horizontal velocities, the vertical component of the momentum equation is taken to be hydrostatic:

$$\frac{\partial p^*}{\partial z^*} = -\rho^* g^* \tag{1.4}$$

Integrating in the vertical:

$$p^* = -\int \rho^* g^* \, dz^* = -\rho^* g^* z^* + \text{constant} \tag{1.5}$$

The constant is evaluated at $z^* = \eta^*$, where the pressure is zero. Then

$$p^* = \rho^* g^* (\eta^* - z^*) \tag{1.6}$$

Linearized surface boundary conditions are applied at $z = 0$:

$$\frac{\partial u^*}{\partial z^*} = \frac{\tau^* \tau_x}{\rho^* K_v^*}, \qquad \frac{\partial v^*}{\partial z^*} = \frac{\tau^* \tau_y}{\rho^* K_v^*}, \qquad p^* = \rho^* g^* \eta^* \qquad \text{and} \qquad w^* = 0 \tag{1.7}$$

where $\tau_x,\ \tau_y$ are the components of the wind stress along x and y. For this problem, the wind stress is taken to blow along the x-axis, with maximum amplitude τ^*. On the bottom, the no-slip condition is enforced.

1.2 Non-dimensional model

Take B^* (the half width) to be a characteristic length. Define the following dimensionless variables:

$$x^* = B^* x, \quad y^* = B^* y, \quad L^* = B^* L \quad z^* = H^* z, \quad u^* = \frac{\tau^* H^*}{\rho^* K_v^*} u, \quad v^* = \frac{\tau^* H^*}{\rho^* K_v^*} v, \quad w^* = \frac{\tau^* H^*}{\rho^* K_v^*} \frac{H^*}{B^*} w \tag{1.8}$$

The choice of scaling for the velocities is based on the surface stress boundary condition, and the mass conservation equation. The non-dimensional parameter L is the horizontal aspect ratio of the basin. Consider the wind to be blowing along the x-axis, with constant strength (from now on, $\tau_s^x = \tau^* \tau(x, y)$ and $\tau_s^y = 0$).

Introducing these non-dimensional terms into equation 1.2 gives:

$$\rho^* g^* \frac{\partial \eta^*}{\partial x^*} = \frac{\rho^* K_v^*}{H^{*2}} \frac{\tau^* H^*}{\rho^* K_v^*} \left(\frac{H^{*2}}{L^{*2}} \frac{\partial^2 u}{\partial x^2} + \frac{H^{*2}}{L^{*2}} \frac{\partial^2 u}{\partial y^2} + \frac{\partial^2 u^*}{\partial z^{*2}} \right); \tag{1.9}$$

If $L^* \gg H^*$ the first two terms inside the parenthesis of equation 1.9 can be neglected since they are much smaller than the third term. Since both the pressure and diffusion terms must balance it is clear that a good choice for non-dimensional surface elevation is

$$\eta^* = \frac{\tau^* L^*}{\rho^* g^* H^*} \eta \tag{1.10}$$

In terms of the new variables, the momentum statement is that the sum of pressure and shear forces is zero: the linearized problem reduces to:

$$\frac{\partial u}{\partial x} + \frac{\partial v}{\partial y} + \frac{\partial w}{\partial z} = 0 \tag{1.11}$$

Equation 1.9 simplifies to:

$$\frac{\partial \eta}{\partial x} = \frac{\partial^2 u}{\partial z^2} \tag{1.12}$$

and after a similar treatment to the y-component of the momentum equation:

$$\frac{\partial \eta}{\partial y} = \frac{\partial^2 v}{\partial z^2} \tag{1.13}$$

The remaining boundary conditions are:

$$\frac{\partial u}{\partial z} = \tau_x, \quad \frac{\partial v}{\partial z} = \tau_y, \quad w = 0 \quad \text{at} \quad z = 0; \quad u = v = w = 0 \quad \text{at} \quad z = -h \tag{1.14}$$

where $h = h^*/H^*$, the *local* non-dimensional depth. In addition, there can be no flow through lateral boundaries.

To find a solution. equations 1.12 and 1.13 are integrated twice in the vertical. After applying the boundary conditions, the solutions are found to be:

$$u = \tau_x(z + h) + \frac{\partial \eta}{\partial x}\frac{z^2 - h^2}{2}, \quad v = \tau_y(z + h) + \frac{\partial \eta}{\partial y}\frac{z^2 - h^2}{2}. \tag{1.15}$$

To better understand these solutions, it is helpful to rewrite the first of equation 1.15 as:

$$\frac{u}{h} = \tau_x \left(\frac{z}{h} + 1\right) + \frac{h}{2}\frac{\partial \eta}{\partial x}\left(\frac{z^2}{h^2} - 1\right) \tag{1.16}$$

The vertical profile of the ratio u/h is shown as a function of z/h in figure 1.2. In this figure the stress $\tau_x = 1$ and the product $h\,\partial\eta/\partial x$ is varied between 0 and 2. If $h\,\partial\eta/\partial x = 0$, the velocity increases linearly from the bottom ($z = -h$), where the no-slip boudary condition forces the velocity to zero, to a maximum at the surface, where $\partial u/\partial z = \tau_x$, as required by the first boundary condition in equation 1.14. This is Poiseuille flow.

As $\partial\eta/\partial x$ increases from zero, the velocities become smaller: a *positive* pressure gradient drives the flow toward *negative* x.

Note also that the velocity profile depends on h. If h is very small, then the second term in the expression for u dominates over the first. In a basin such as the one illustrated in figure 1.1 the flow on the shallow sides one expects the flow to be like Couette flow.

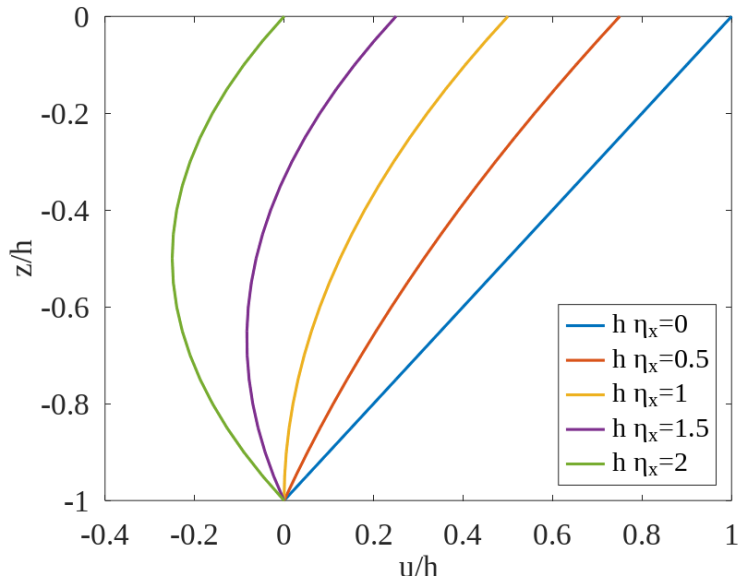

Figure 1.2: Vertical velocity profiles for $\tau_x = 1$, and various choices of $h\eta_x$. When $\eta_x = 0$ the solution is Poiseuille flow. For other values of $h\eta_x$, the solutions are a combination of Poiseuille and Couette flow

1.3 The transport

Define the components of the horizontal transport as

$$[u] = \int_{-h}^{0} u\, dz = \tau_x \frac{h^2}{2} - \frac{\partial \eta}{\partial x}\frac{h^3}{3} \tag{1.17}$$

where the terms on the right result from vertically integrating equation 1.15 from the bottom ($z = -h$) to the surface ($z = 0$).The first term shows that wind stress forces transport downwind, while the second term shows a positive pressure gradient forces transport upwind. This makes it clear that the vertically integrated transport is governed by a balance betwwen stress and

elevation gradient. A similar result is found for the lateral transport (v):

$$[v] = \int_{-h}^{0} v\, dz = \tau_y \frac{h^2}{2} - \frac{\partial \eta}{\partial y}\frac{h^3}{3} \tag{1.18}$$

An equation relating the two components of transport can be derived by integrating the mass conservation 1.11 equation from the bottom to the surface:

$$\int_{-h}^{0} \frac{\partial u}{\partial x}\, dz + \int_{-h}^{0} \frac{\partial v}{\partial y}\, dz + w|_0 - w|_{-h} = 0 \tag{1.19}$$

The vertical velocity is zero at the surface and at the bottom, so the last two terms on the left of equation 1.19 are zero. The order of integration and differentiation in equation 1.19 can be interchanged, and the vertically velocity is zero both at the bottom and surface of the fluid, so the tranport field is divergence free:

$$\frac{\partial [u]}{\partial x} + \frac{\partial [v]}{\partial y} = 0 \tag{1.20}$$

At this point there are two equivalent ways to proceed.

1.3.1 An equation for sea level η

Substituting equations 1.17 and 1.18 into equation 1.20 leads to a second order partial differential equation for the sea level:

$$\frac{\partial}{\partial x}\left(h^3 \frac{\partial \eta}{\partial x}\right) + \frac{\partial}{\partial y}\left(h^3 \frac{\partial \eta}{\partial y}\right) = \frac{\partial}{\partial x}\left(\tau_x \frac{3h^2}{2}\right) + \frac{\partial}{\partial y}\left(\tau_y \frac{3h^2}{2}\right) \tag{1.21}$$

with the boundary condition of no transport normal to a boundary. Since the transport is related to the surface level gradients through equations 1.17 and 1.18. The boundary conditions on gradients in η are:

$$h\frac{\partial \eta}{\partial x} = \frac{3}{2}\tau_x, \quad \text{at} \quad x = \pm L; \quad h\frac{\partial \eta}{\partial y} = \frac{3}{2}\tau_y, \quad \text{at} \quad y = \pm 1 \tag{1.22}$$

1.3.2 An equation for the streamfunction ψ

Since the transport velocities are divergence free, they cab be expressed in terms of a single variable, $\psi(x, y)$ called the tranport streamfunction:

$$[u] = -\frac{\partial \psi}{\partial y} \quad [v] = \frac{\partial \psi}{\partial x} \tag{1.23}$$

This definition implies that the transport (vertically integrated velocity) follows lines of constant ψ and that the distance between streamlines is related to the magnitude of the transport: where streamlines are bunched together the transport is relatively large and vice-versa. Since there can be no transport across a boundary, streamlines cannot end on a boundary. As a consequenvce the streamfunction ψ must be constant along a solid boundary and that constant is often taken to be zero.

Equations 1.17 and 1.18 can be re-written to express the surface level gradients in terms of transports and the forcing:

$$\frac{\partial \eta}{\partial x} = \tau_x \frac{3}{2h} + \frac{3}{h^3}\frac{\partial \psi}{\partial y}, \qquad \frac{\partial \eta}{\partial y} = \tau_y \frac{3}{2h} - \frac{3}{h^3}\frac{\partial \psi}{\partial x} \tag{1.24}$$

Cross differentiating and subtracting equations 1.24 to eliminate the surface level gradients gives:

$$\frac{\partial}{\partial x}\left(\frac{1}{h^3}\frac{\partial \psi}{\partial x}\right) + \frac{\partial}{\partial y}\left(\frac{1}{h^3}\frac{\partial \psi}{\partial y}\right) = \frac{\partial}{\partial x}\left(\frac{\tau_y}{2h}\right) - \frac{\partial}{\partial y}\left(\frac{\tau_x}{2h}\right) \tag{1.25}$$

The boundary condition is simply that the streamfunction be equal to zero along all boundaries. Practically this implies that solutions for ψ are much easier to find that solutions for η. If the boundary includes an opening (as in the case of a bay or estuary), the direction of the flow through the opening can be specified.

1.4 The Solution

Finding the three components of the local velocity at each location in a three-dimensional basin directly can be done by proceeding in steps:the local velocities are known functions of the bathymetry and surface level gradients. The surface level (and the streamfunction) are single variables that are functions of x and y only. This opens the possibility of first finding η or ψ in the region near mid-basin. Once these are known, the local velocities are determined by equation 1.15.

1.4.1 Solution near mid-basin

For simplicity, consider first a basin such as is illustrated in figure 1.1, where a wind stress is applied in the direction of $+x$ ($\tau_x = 1$, $\tau_y = 0$). Focus on the region near the middle of the basin, $x \approx 0$, where ψ is expected to depend only on y: the transport streamlines are aligned with the basin sidewalls. Given the definition of ψ, equation 1.23, equation 1.17 can be written:

$$\frac{\partial \psi}{\partial y} = -\frac{\tau_x h^2}{2} + \frac{\partial \eta}{\partial x}\frac{h^3}{3} \tag{1.26}$$

where the wind stress is assumed to be constant

If the basin is closed, the streamfunction must have the same values on both sides of the basin ($y = \pm 1$), setting the laterally averaged transport to zero gives:

$$\psi|_{y=1} - \psi|_{y=-1} = -\frac{\tau_x}{2}\int_{-1}^{1} h^2\, dy + \frac{1}{3}\frac{\partial \eta}{\partial x}\int_{-1}^{1} h^3\, dy = -\frac{\tau_x}{2}\left\langle h^2 \right\rangle + \frac{\partial \eta}{\partial x}\frac{\langle h^3 \rangle}{3} \tag{1.27}$$

where the <> brackets denote integrals across the width of the basin. Far from the up and downwind ends, the axial surface level gradient is:

$$\frac{\partial \eta}{\partial x} = \frac{3\tau_x}{2}\frac{\langle h^2 \rangle}{\langle h^3 \rangle} \tag{1.28}$$

If, for instance the bottom profile is a linear trough, that is $h = 1 - |y|$, then $< h^2 >= 1/3$ and $< h^3 >= 1/4$, and $\partial\eta/\partial x = 2\tau_x$. The streamfunction ψ and the axial transport $[u]$ are illustrated as a function of lateral position y at $x = 0$ in Fig. 1.3.

Knowing τ_x and $\partial\eta/\partial x$, the local axial velocity is given by equation 1.15. Near mid-basin, the lateral velocity $v = 0$ because both $\tau_y = 0$ and $\partial\eta/\partial y = 0$. Only the axial velocity u is non-zero. Figure 1.4 shows contours of u drawn for a section across the basin located at $x = 0$. Areas wher the axial velocity is upwind (in the opposite direction from τ_x) are shaded. Downwind flow is found near the sides of the basin, where the flow is closer to Poiseuille flow.

In Chapter 6 of his book, on page 92 Arnoldo shows similar maps of u for different basin shapes. While details of the velocity distribution vary, the qualitative result, that fluid flows downwind over shallow areas and upwind in the deeper areas remains unchanged.

Returning to dimensional values, one should ask how large can these parameters can be in a practical situation. How big is this? Imagine the wind is 10 ms^{-1}, this corresponds to $\tau^* = 0.1$ Pa, say the lake is $H^* \approx 10$ m deep and a typical length is

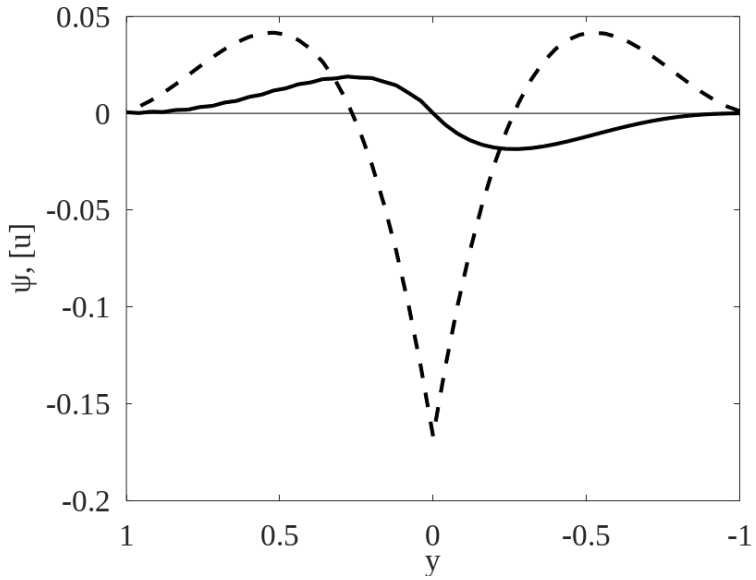

Figure 1.3: Two-dimensional transport streamfunction ψ (solid line), and the corresponding transport $[u] = -\psi_y$ (dashed) as a function of lateral position at mid-basin for a linear bottom slope. The observer is looking toward $+x$, so the y axis points to the left. In shallow depths, the transport $[u]$ is downwind (Poiseuille flow). For this

$L^* \approx 10\ km$.

$$\eta^*_{x^*} = 2\frac{0.1}{1000 \times 10 \times 10} = 2\ 10^{-6} \tag{1.29}$$

if the half length of the lake is taken a 5 km, the surface lever rise (or fall)t at the end of the lake is $\eta^* = 2 \times 10^{-6} \times 5 \times 10^3$ or about one centimeter. Because $\tau^* H^*/(\rho^* K^*_v) \approx 1$ dimensional values of the axial velocity have comparable magnitude as the non-dimensional values. Typically a wind stres $\tau^* \approx 0.1\ Pa$ drives currents of near 0.1 ms^{-1}

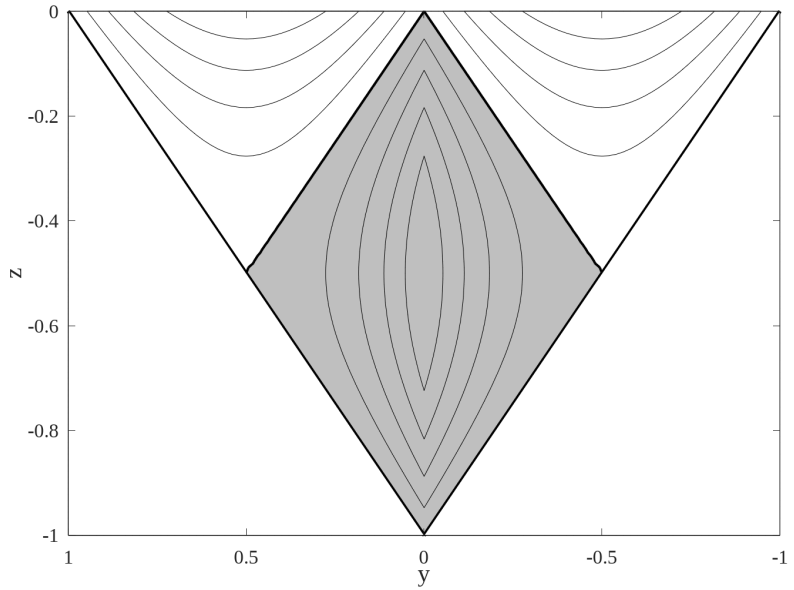

Figure 1.4: The axial velocity $u(y, z)$ near mid-basin for a constant wind stress blowing toward $+x$. Shaded areas are negative (upwind) values of u; unshaded areas (downwind) correspond to positive values. Fluid flows in the same direction as the wind stress in the shallow portion of the basin, and the return flow is concentrated in the deeper parts. The contour increment is 0.05. Note the similarity with Arnoldo's figure 6.3a, in his book.

1.4.2 Solution for the full basin

Near the ends of the basin ($|x| \approx L$), the downwind flow must turn and connect to the upwind flow. A solution for the streamfunction in the entire basin, based on normal modes, has been proposed by **?**. The solution for both the transport streamfunction ψ and the surface level η is included in my notes on normal modes `Projects/Maths/Normal_Modes/NM.pdf`.

The solutions for the transport streamfunction, ψ, and the sea level η, driven by a unit wind stress acting along $+x$, are

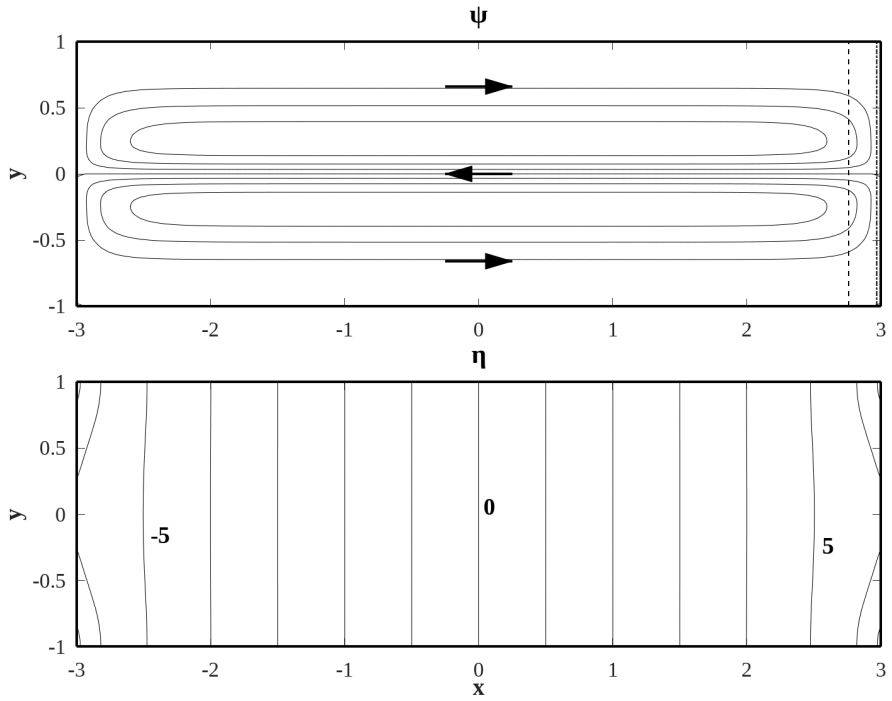

Figure 1.5: The transport streamfunction ψ, driven by a unit wind stress directed toward $+x$, is illustrated on the top. The contour interval is $5\,10^{-3}$. Arrows indicate the direction: the tranport on the shallow sides is in the same direction as the wind stress, toward the right of the page. The return transport take place in a narrow concentrated core in the vicinity of $y = 0$.The dashed and dot-dash lines locate the sections illustrated in figure 1.6. The sea level η is illustrated in the lower panel (contour interval is 1): over most of the basin η rises downind with a slope $\partial\eta/\partial x = 2$, in the sense to oppose the wind stress.

illustrated in figure 1.5.

The pattern for ψ (top frame) consists of two closed gyres, symmetric about the x-axis. The arrows indicate the direction

of motion for the case when the wind is blowing toward the left of the figure. As described above, the transport is downwind in the shallow areas, where $|y| \approx 1$. Near the ends of the basin, $x \approx L$, the streamlines bend, to allow the tranport to turn and join the central (near $y = 0$) core where fluid returns upstream. This core is show as the shadded area in figure 1.4.

The sea level η (bottom frame of figure 1.5) slopes up toward the right over most of the basin. Away from the corners the slope of the sea level $\partial\eta/\partial x = 2$, as expected from equation 1.28. Sea level behaves differently near the corners rising to peaks on the downwind end ($x \approx L$), and large negative values on the upwind end ($x \approx -L$). The maxima nad minima supply the relative large pressure gradients required to turn the flow away from the sides and toward the central core on the downwind end, with the reverse occurence on the upowind end.

Local velocities (u, v, and w).

Given the transport ψ and the forcing τ, the surface level gradients $\partial\eta/\partial x$ and $\partial\eta/\partial y$ are given by equation 1.24. The surface level gradients and the applied wind stress then determine the horizontal components of velocity, as given in equation 1.15.

To get the vertical velocity, start from the continuity equation 1.11:

$$\frac{\partial w}{\partial z} = -\frac{\partial u}{\partial x} - \frac{\partial v}{\partial y} = -\frac{z^2 - h^2}{2}\left(\frac{\partial^2\eta}{\partial x^2} + \frac{\partial^2\eta}{\partial y^2}\right) + h\frac{\partial h}{\partial y}\frac{\partial \eta}{\partial y} \tag{1.30}$$

In the case considered here, when the wind stress in constant and the depth only a function of y, equation 1.21 can be written:

$$\frac{\partial^2\eta}{\partial x^2} + \frac{\partial^2\eta}{\partial y^2} = -\frac{3}{h}\frac{\partial h}{\partial y}\frac{\partial \eta}{\partial y} \tag{1.31}$$

substituting into equation 1.30

$$\frac{\partial w}{\partial z} = \frac{3}{h}\frac{\partial h}{\partial y}\frac{\partial \eta}{\partial y}\frac{z^2 - h^2}{2} + h\frac{\partial h}{\partial y}\frac{\partial \eta}{\partial y} = \frac{h}{2}\frac{\partial h}{\partial y}\frac{\partial \eta}{\partial y}\left(3\frac{z^2}{h^2} - 1\right) \tag{1.32}$$

Upon integration this gives

$$w = \frac{\partial h}{\partial y}\frac{\partial \eta}{\partial y}\frac{z}{2h}\left(z^2 - h^2\right) \tag{1.33}$$

which satisfies the boundary condition that $w = 0$ at both the bottom ($z = -h$) and the surface ($z = 0$).

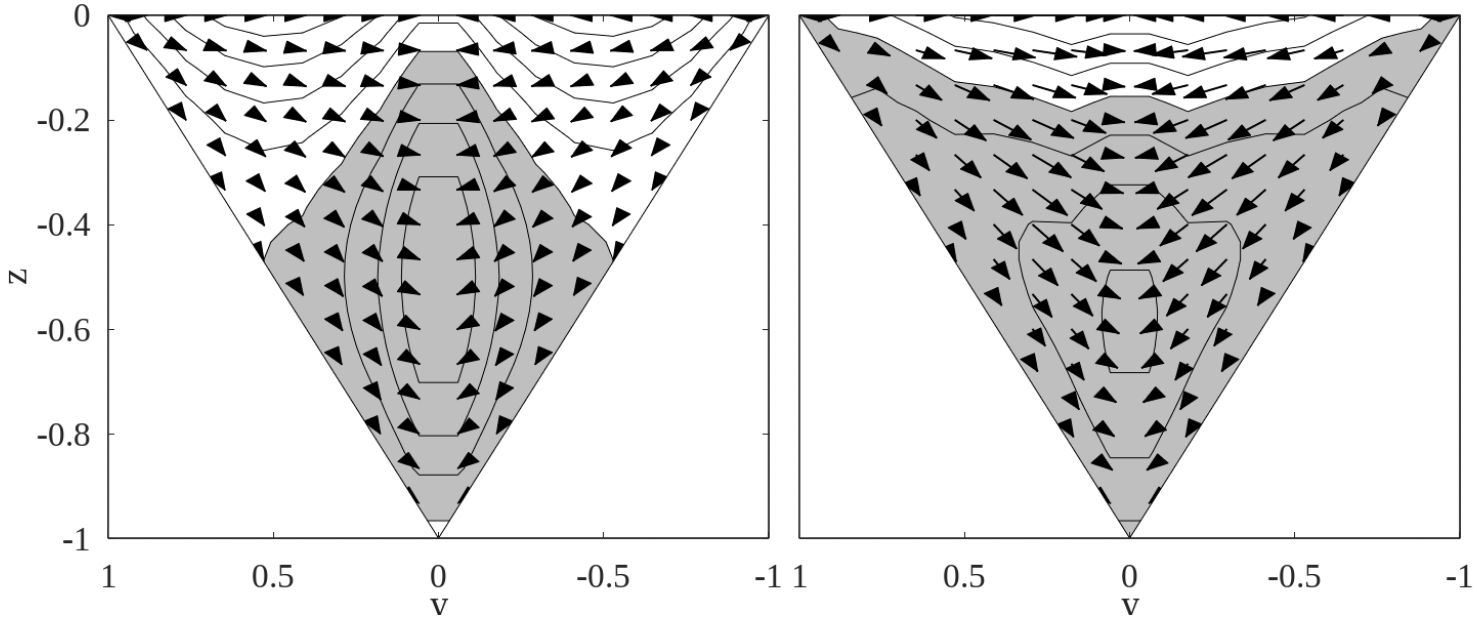

Figure 1.6: Sections showing the three local velocities (u, v, w) across the channel at $x = 2.76$ and $x = 2.97$. The shading is as in figure 1.4: the axial velocity is smaller in both these sections than at mid-basin. The lateral and vertical velocities are (both zero near the middle of the basin) reflect the convergence of flow toward the center and botoom of the basi. This is where the surface downwind flow turns the join the deep upwind transport

Over most of the basin the lateral (v) and vertical (w) are zero. The flow is axial, as illustrated in figure 1.4. Near the basin end (at $x = \pm 3$), the flow needs to turn and v and w become comparable to u. This is illustrated in the two sections shown in figure 1.6, at located at $x = 0.92$ and at $x = 0.99$. The axial velocity id positive near the urface and negative near the bottom. The lateral velocity transports some of this fluid toward the center of the basin and the vertical velocity transports fluid down, wher it is caught up in the upwind return.

1.5 Realistic Topography

In all the cases dealt with to this point, the topography has been idealized, consiting of rectangular basins with smoothly varying bathymetry. In this section the theory is used to describe the circulation in Bahia Concepción, located on the western shore of the surface of Cortez. The bay, illustrated in figure 1.7 is located on the western side on the Gulf of California. The greatest depths are about $30\,m$ (left panel, figure 1.7).

The transport streamfunction ψ has been found by solving equation 1.25 using the finite element method (see my FEM notes). The transport streamfunction is show on the right panel of figure 1.7. According to the model decribed in the chapter, wid toward to southeast should result in transport in the same direction along the sides of the bay, with a concentrated subsurface return in the deeper part of the basin. Drifter observation in the bay are consistent with the occurence of downwind transport on the left side of the bay, however the return appears to take place closer to the other side, leaving a broad circular Cyclonic gyre near the closed end.

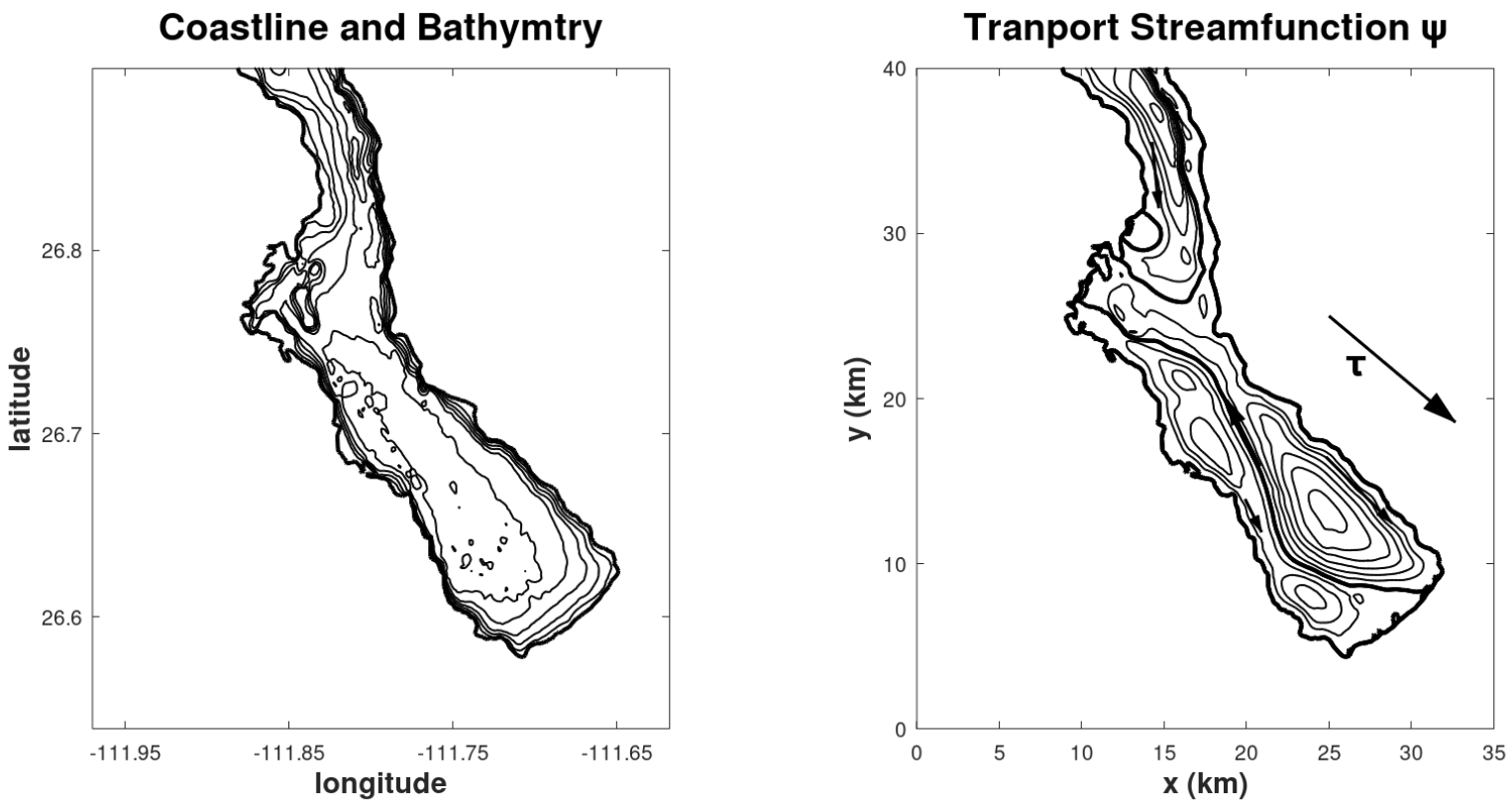

Figure 1.7: Bahia Concepción. Left: Bathymetry (m); contours are drawn at $5\,m$ interval. The greatest depth in the southern part of the Bay is about $30\,m$.; Right: Transport streamlines. The wind blows toward the SE, as shown by the arrow to the right of the transport map. Arrowheads on the streamlines show the direction of the transport: into the bay on the sides with return near the center.

Chapter 2

A shallow wind-driven lake on the f-plane

2.1 The model

In this chapter, the model described in Chaprter 1 is extended to include the effects of the rotation of the earth. When the Coriolis effect is accounted for th steady, linearized momentum equations so that equation 1.2 and 1.3 become:

$$-f^* v^* = -\frac{\partial p^*}{\partial x^*} + \rho^* K_v^* \left(\frac{\partial^2 u^*}{\partial x^{*2}} + \frac{\partial^2 u^*}{\partial y^{*2}} + \frac{\partial^2 u^*}{\partial z^{*2}} \right); \tag{2.1}$$

$$f^* u^* = -\frac{\partial p^*}{\partial y^*} + \rho^* K_v^* \left(\frac{\partial^2 v^*}{\partial x^{*2}} + \frac{\partial^2 v^*}{\partial y^{*2}} + \frac{\partial^2 v^*}{\partial z^{*2}} \right) \tag{2.2}$$

In this problem, inclusion of the Coriolis acceleration ($f^* = 2\Omega \sin\lambda \approx 10^{-4} s^{-1}$) is shown to fundamentally alter the flow described in the previous problem. In particular, with the wind still blowing toward positive x, the surface level now tilts in both the axial and the lateral direction, in order to balance the Coriolis acceleration. This has profound implications in terms of the circulation.

2.2 Non-dimensional model

Using the same non-dimensional variables as were defined in 1.8, the mass conservation equation 1.11 is unchanged, and the momentum equations acquire an additiona term due to rotation:

$$\frac{\partial^2 u}{\partial z^2} + \frac{2}{\delta_E^2} v = \frac{\partial \eta}{\partial x} \tag{2.3}$$

and

$$\frac{\partial^2 v}{\partial z^2} - \frac{2}{\delta_E^2} u = \frac{\partial \eta}{\partial y}. \tag{2.4}$$

The parameter $\delta_E = 2K^*/(f^* H^{*2})$ represents the ratio of the Ekman layer thickness to the maximum depth H^* of the basin. Without rotation, $\delta_E \to \infty$, and the viscous effects are spread throughout the fluid layer (fully developed flow) as in Chapter 1. When the Coriolis acceleration is included in the analysis, the viscous effects are confined within boundary layers of order δ_E. Typically, at mid-latutudes the Ekman layer thickness is of order 10 m. The boundary conditions themselves are unchanged from equation 1.14 in the previous chapter.

This system of ordinary differential equations 2.3 and 2.4 can be solved for the horizontal velocities:

$$u(z) = q^\tau(z)\tau_x - r^\tau(z)\tau_y + q^\eta(z)\frac{\partial \eta}{\partial x} - r^\eta(z)\frac{\partial \eta}{\partial y} \tag{2.5}$$

$$v(z) = q^\tau(z)\tau_y + r^\tau(z)\tau_x + q^\eta(z)\frac{\partial \eta}{\partial y} + r^\eta(z)\frac{\partial \eta}{\partial x} \tag{2.6}$$

where $\gamma^2 = 2\mathrm{i}/\delta_E^2$ and

$$q^\tau + ir^\tau = \frac{\sinh\gamma(z+h)}{\gamma\cosh\gamma h}, \quad q^\eta + ir^\eta = \frac{1}{\gamma^2}\left(\frac{\cosh\gamma z}{\cosh\gamma h} - 1\right); \tag{2.7}$$

Equations 2.5 through 2.6 set the vertical structure of the horizontal velocities when rotation is taken into account. As $\delta \to \infty$ they become equal to equations 1.15. However when δ is finite the solutions are very different from the non-rotating case: the most obvious difference being that wind stress or sea elevation gradients drive currents in *both* the direction of the applied force *and* the direction perpendicular to the applied force. This is a direct result of the Coriolis accelerations in equations 2.3 and 2.4.

The functions q^τ, r^τ (left panel of figure 2.1) represent the vertical structure of both velocity components to a unit wind stress ($\tau_x = 1$). In the vertical, the response does not penetrate all the way to the bottom, rather it is confined near the surface in a layer of thickness δ (in this case $\delta = 2$), called the Ekman layer.

The response to a unit sea level gradient is given by q^η, r^η, (right panel of figure 2.1). Again both components respond, and the velocity changes in a region near the bottom, another Ekman layer.

When rotation is ignored the fluid responds throughout the water column, in the direction of the imposed forcing. The result described here is profoundly different: wind stress and sea level gradients drive flow in two directions, in relatively narrow Ekman layers, near the surface and the bottom. In between, a region called the interior, the flow is uniform, if a pressure gradient exists it is in geostropic equilibrium with a current at right angles to the forcing.

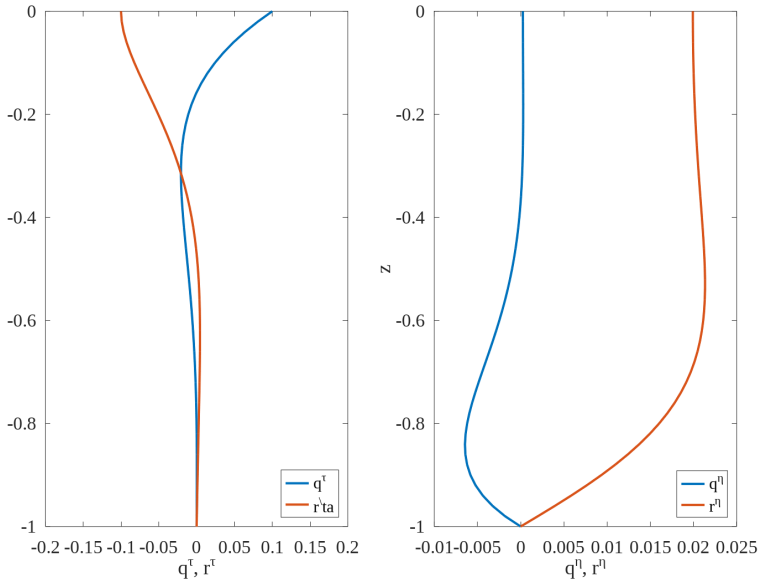

Figure 2.1: Local velocity profiles for $\delta = 0.2$. Left: vertical response of velocity to a unit wind stress in the $+x$ direction; q^τ (blue),and r^τ (red). Right: vertical response of velocity to a unit elevation gradient in the $+x$ direction; q^η (blue),and r^η (red)

2.3 The transport

The relation between transports $[u]$, $[v]$ and the forcings are found by integrating equations 2.5 and 2.6 from the bottom to the surface:

$$[u] = Q^\tau \tau_x - R^\tau \tau_y + Q^\eta \frac{\partial \eta}{\partial x} - R^\eta \frac{\partial \eta}{\partial y} \tag{2.8}$$

$$[v] = Q^\tau \tau_y + R^\tau \tau_x + Q^\eta \frac{\partial \eta}{\partial y} + R^\eta \frac{\partial \eta}{\partial x} \tag{2.9}$$

where

$$Q^\tau + iR^\tau = \frac{1}{\gamma^2} \frac{\cosh \gamma h - 1}{\cosh \gamma h}, \quad Q^\eta + iR^\eta = \frac{1}{\gamma^3} \left(\tanh \gamma h - \gamma h \right); \tag{2.10}$$

Just as with the velocities, transports also depend on *both* components of the pressure gradient and stress. comparing equations 2.8 and 2.9 with equations 1.17 and 1.18: it is apparent that the parameters Q^τ, R^τ, Q^η, R^η here play the same role as depth raised to some power in the no-rotation case. Limiting forms for these four parameters are given below.

2.3.1 An equation for sea level

As in the previous problem, introducing equations 2.8 and 2.9 into the vertically integrated mass conservation equation yields a second oder elliptic PDE for η:

$$\frac{\partial}{\partial x} \left(Q^\eta \frac{\partial \eta}{\partial x} - R^\eta \frac{\partial \eta}{\partial y} \right) + \frac{\partial}{\partial y} \left(Q^\eta \frac{\partial \eta}{\partial y} + R^\eta \frac{\partial \eta}{\partial x} \right) = \frac{\partial}{\partial x} \left(R^\tau \tau_y - Q^\tau \tau_x \right) - \frac{\partial}{\partial y} \left(R^\tau \tau_x - Q^\tau \tau_y \right) \tag{2.11}$$

The boundary condition states that there can be no transport (as defined in equations 2.8 and 2.9) normal to a boundary. These boundary conditions are not homogeneous, and are more difficult to enforce that the boundary condition on the transport streamfunction.

2.3.2 An equation for the streamfunction

Equations 2.8 and 2.9 can be re-written to express the surface level gradients in terms of transports and the forcing:

$$\frac{\partial \eta}{\partial x} = A\frac{\partial \psi}{\partial y} - B\frac{\partial \psi}{\partial x} + C\tau_x - D\tau_y, \qquad \frac{\partial \eta}{\partial y} = -A\frac{\partial \psi}{\partial x} - B\frac{\partial \psi}{\partial y} + C\tau_y + D\tau_x \tag{2.12}$$

where the transport streamfunction ψ is defined as before (equation 1.23) and

$$A = -\frac{Q^\eta}{Q^{\eta 2} + R^{\eta 2}}; \quad B = -\frac{R^\eta}{Q^{\eta 2} + R^{\eta 2}} \quad C = -\frac{Q^\eta Q^\tau + R^\eta R^\tau}{Q^{\eta 2} + R^{\eta 2}} \quad D = \frac{Q^\tau R^\eta - Q^\eta R^\tau}{Q^{\eta 2} + R^{\eta 2}} \tag{2.13}$$

The four parametrs A, B, C, and D are also functions of local depth $h(x, y)$ and δ. Cross differentiating and subtracting equations 2.12 gives

$$\frac{\partial}{\partial x}\left(A\frac{\partial \psi}{\partial x} + B\frac{\partial \psi}{\partial y}\right) + \frac{\partial}{\partial y}\left(A\frac{\partial \psi}{\partial y} - B\frac{\partial \psi}{\partial x}\right) = \frac{\partial}{\partial x}\left(C\tau_y + D\tau_x\right) - \frac{\partial}{\partial y}\left(C\tau_x - D\tau_y\right) \tag{2.14}$$

The boundary condition is simply that the streamfunction be equal to zero along the boundary. This equation was first derived by **?**.

2.3.3 Limits

When friction is large and rotation is weak, the so-called fully developed flow,: ($\delta \to \infty$),

$$Q^\eta + iR^\eta \to -\frac{h^3}{3} \quad Q^\tau + iR^\tau \to \frac{h^2}{2} \tag{2.15}$$

$$A \to \frac{3}{h^3}, \quad B \to 0, \quad C \to \frac{3}{2h}, \quad D \to 0. \tag{2.16}$$

The equation for ψ reduces to equation 1.25

When friction is small and rotation is large ($\delta \to 0$),

$$Q^\eta + iR^\eta \to -\frac{\delta^3}{4} + i\frac{\delta^2 h}{2} \quad Q^\tau + iR^\tau \to -i\frac{\delta^2}{2}. \tag{2.17}$$

$$A \to -\frac{1}{\delta h^2}, \quad B \to -\frac{2}{\delta^2 h}, \quad C \to -\frac{1}{h}, \quad D \to -\frac{\delta}{2h^2}. \tag{2.18}$$

2.4 The Solution

As in the previous chapter, the solution away from the end id dicussed first, because of the relative simplicity of the problem. The solution near the ends is described later.

2.4.1 Solution near mid-basin

Away from the up/downwind ends, if h and related parameters depend only on y, and if the wind stress is parallel to the x-axis ($\tau_x = 1\, \tau_y = 0$) equation 2.14 reduces to:

$$\frac{\partial}{\partial y}\left(A\frac{\partial \psi}{\partial y}\right) = -\frac{\partial C}{\partial y}. \tag{2.19}$$

Equation 2.19 can be integrated once to give:

$$\frac{\partial \psi}{\partial y} = \frac{1}{A}\left(\frac{< C/A >}{< 1/A >} - C\right) \tag{2.20}$$

where A and C are the functions defined in equation 2.13. The solution for the transport streamfunction ψ and the transport $[u] = -\psi_y$ are illustrated in figure 2.2. The only difference between figure 2.2 and figure 1.3 is the amplitude of the transport, smaller when rotation is included in the analysis. This is because rotation limits the magnitude of the velocities.

Again, near mid-basin, $\partial\eta/\partial x$ is independent of y, and $[v] = 0$. If $\tau_y = 0$, equation 2.9 gives $\partial\eta/\partial y$ as a function of $\partial\eta/\partial x$:

$$\frac{\partial \eta}{\partial y} = -\frac{1}{Q^\eta}\left(R^\tau \tau_x + R^\eta \frac{\partial \eta}{\partial x}\right), \tag{2.21}$$

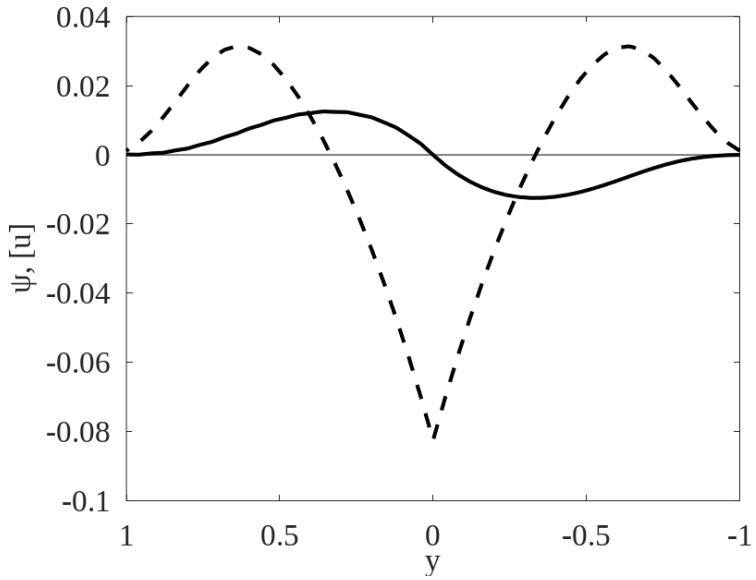

Figure 2.2: Same as figure 1.3, but including rotation, with $\delta = 1/6$.

which can be substituted into equation 2.8 and averaged across the width of the basin:

$$[u] = Q^\tau \tau_x + Q^\eta \frac{\partial \eta}{\partial x} + \frac{R^\eta}{Q^\eta}(R^\tau \tau_x + R^\eta \frac{\partial \eta}{\partial x}) = \left(Q^\tau + \frac{R^\eta}{Q^\eta} R^\tau\right) \tau_x + \left(Q^\eta + \frac{R^\eta}{Q^\eta} R^\eta\right) \frac{\partial \eta}{\partial x} \tag{2.22}$$

Take the lateral average of the terms in equation 2.22. Since the lateral average of the axial transport must be zero ($< [u] >= 0$), the surface elevation gradient must be:

$$\frac{\partial \eta}{\partial x} = -\frac{\langle Q^\tau + R^\eta \, R^\tau / Q^\eta \rangle}{\langle Q^\eta + R^{\eta 2} / Q^\eta \rangle} \tau_x \tag{2.23}$$

This is exactly the same reasoning that led to equation 1.28 in the previous chapter.

2.4.2 Solution for the full basin.

To find ψ throughout the basin, equation 2.14 needs to be solved, with the boundary condition that $\psi = 0$ on all the sides of the basin. An analytical solution in an idealized basin is included in **?**. Here a numerical solution, based on the finite element method (FEM) is described. The advantage of the FEM is that it can be applied in an arbitrarily shaped domain, and can accomodate both open and fixed boundary conditions.

This solution is illustrated in figure 2.3 for $\delta = 1/6$, in a basin where $L = 3$ and the depth is a linear function of y: $h = 1 - |y|$. Near mid-basin ($x \approx 0$) the streamline pattern in this case is similar to ψ in the non-rotating case (top panel in figure 1.5), the only discernable difference near mid-basin ($-1 \leq x \leq 1$) being in the amplitude, which is smaller in the rotating case, as explained above.

The similarity with the non-rotating case is no longer true near the basin ends. One obvious difference is that the turning regions at either end in figure 2.3 are different depending on which side of the basin one is looking at: on the right side ($x \approx 3$) the turning region in the negative y half-plane is smaller tha on the positive y half-plane. This asymmetry is esplained by different dynamical balances governing the flow where the bottom slope is positive or negative, as explained in **?**. The reverse is true on the left end ($x \approx -3$) where the tight turning is found on the positive y half-plane, and the more gardual turning on the other side.

Given ψ, surface elevation gradients can be evaluated using equations 2.12. Then the local velocities can be detrmined for equation 2.5 and 2.6. The vertical velocity is then determined by integrating the mass conservation equation down from the surface, as was done in the previous chapter (see equation 1.30).

The local velocities computed along two sections, one located at $x = 0$ and the other at $x = 2.9$ are illustrated in figure 2.4. Comparing the first of these two sections (left panel of figure 2.4), near mid-basin, to its counterpart in the previous chapter (figure 1.4) it is immediately apparent that while, when rotation is ignored, the only non-zero velocity is axial (u), there is a rich structure in the v and w velocities when the Coriolis acceleration is included in the analysis. In the mid-basin section, the lateral, v velocities can be described in terms of three layers: two Ekman layers covering the top and lower portion of the water column where the lateral flow is to the right of the applied wind stress. These frictional layers are separated by a region, often referred to as the interior, where the lateral velocity is to the left of the wind stress. The flow near the bottom on the left is said to be upwelling, and the near bottom flow on the right is downwelling. In open coastal areas with winds blowing parallel to the coast are usually nutrient rich because of the upwelling.transport. The overal lateral circulation can can be thought of as consisting of two superpose gures: The gyre closest to the surface roates in the clockwise direction (in the Norther hemisphere)

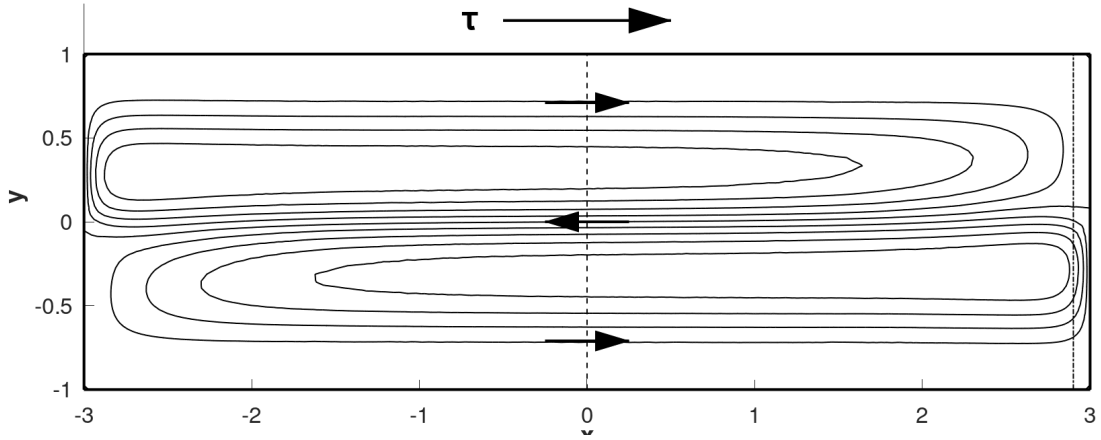

Figure 2.3: The transport stream function ψ obtained using the FEM for $\delta = 1/6$. The wind stress is applied in the $+x$ direction. The streamfunction is zero on the boundaries. The contour interval is $2.5\,10^{-3}$. Compare to top panel in figure 1.5.

and the lower gyre rotates in the opposite sense, driven by veering in the bottom Ekman layer.

Near the closed ends ($|x| \approx 3$), the local velocity pattern (illustred on the right side of figure 2.4) is qualitatively different from what takes place in the mid-basin region. The axial velocity is organized in horizontal layers, with downwind flow near the surface overlying weak upwind flow. The lateral velocities are larger than in any other part of the basin and are larger on the right (negative y) side, where the vertically integrated flow is toward the center of the basin. On the left side, the lateral flow is weaker, which is consistent with the more gradual turning process associated with the broader turning area. Except near the core of the basin, the vertical velocities are negative, and they are larger on the right side. Fluid coming from the central part of the basin to this area arrives near the surface and is swept down and toward the center, where it reverses direction and moves back upwind.

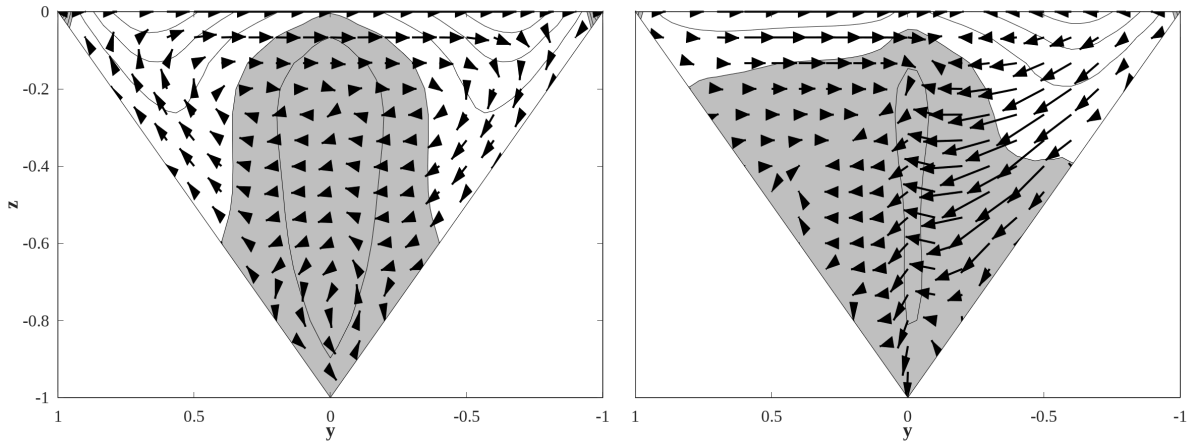

Figure 2.4: Local velocity sections at: left: $x = 0$ (central dashed line in figure 2.3); right: $x = 2.9$ (dot-dash line).

2.5 More realistic basins.

The basin considered so far in this chapter, a trough with triangular cross section is highly idealized. In this section the transport streamfunction computed with the FEM in Bahia Concepción is described. The bathymetry and coastline of Bahia Concepción is shown in the left panel of figure **??**. The transport streamfunction for the case without rotation for a wind angle of 40° i shown in the right panel of the same figure.

The transport streamline pattern, when rotation is included in the analysis ($\delta = 1/6$), is illustrated in figure **??**, for ten values of the wind orientation. In the first plot (upper left) the wind is blowing directly toward the east; in each succesive map the wind orientation is incremented by 10°. In the last plot the wind is toward the south. During the winter and spring, the actual wind orientation usually lies in this quadrant.

The streamline patternss shown in figure 2.5 are sensitive to the orientation of the wind stress. For orientation between 0° (toward the east, up to 40° (top row of maps)the zero level contours divide the bay into three separate zones. In each zone there is a closed circulation that would prevent flow form the closed end from reaching the Gulf of California directly. When the wind direction in more toward the south, the sero level streamline lies on a direct path from the Gulf to the closed end of

the bay.

Where the sero level streamline runs to the shore is also sensity to wind orientation:

2.5.1 Trajectories

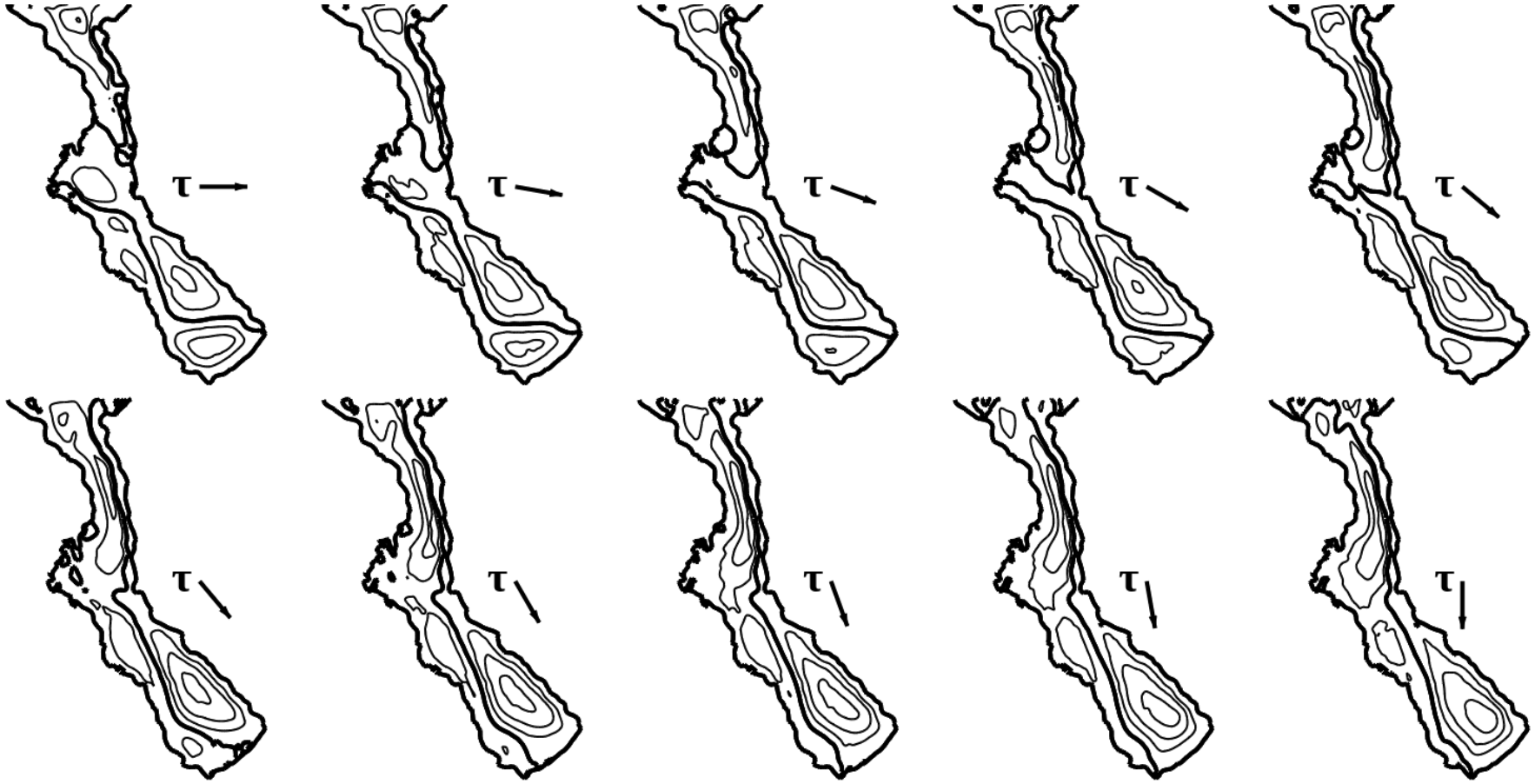

Figure 2.5: The transport streamfunction ψ for ten different wind orientations. The $\psi = 0$ streamline is indicated by a heavier line, and the contour interval 0.1. In the upper leftmost plot, the wind vector is toward the east. In the lower right corner the wind direction is toward the south. The wind direction changes by 10° between plots. In all cases $\delta = 1/6$. The comparable case without rotation is illustrated in the right side frame of figure 1.7

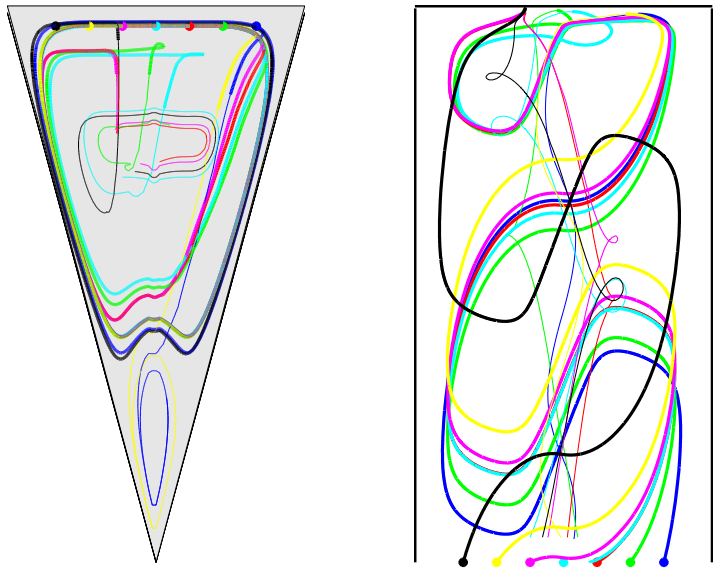

Figure 2.6: Trajectories of several particles released near the surface, at the center ($x = 0$) of a basin, into the $x > 0$ section. The wind is blowing in the $+x$ direction, from the bottom of the page toward the top in the right frame. In the left frame, the viewer is looking along the positive x axis, down the central axis of the basin, toward the closed end. The right hand image is a plan view, from above the basin. The solid symbol marks the release position. The heavy line indicates the trajectory from the release to the furthest inward position, and the light line marks the return trajectory.